

An Emerging Class of Gamma-Ray Flares from Blazars: Beyond One-Zone Models

M. Tavani^{1,2,3}, V. Vittorini¹, A. Cavaliere^{1,2}

Submitted to the *Astrophysical Journal*: July 23, 2015. Accepted: October 13, 2015

ABSTRACT

Blazars radiate from relativistic plasma jets with bulk Lorentz factors $\Gamma \sim 10$, closely aligned along our line of sight. In a number of blazars of the Flat Spectrum Radio Quasar type such as 3C 454.3 and 3C 279 gamma-ray flares have recently been detected with very high luminosity and little or no counterparts in the optical and soft X-ray bands. They challenge the current one-zone leptonic models of emissions from within the broad line region. The latter envisage the optical/X-ray emissions to be produced as synchrotron radiation by the same population of highly relativistic electrons in the jet that would also yield the gamma rays by inverse Compton up-scattering of surrounding soft photons. To meet the challenge we present here a model based on primary synchrotron photons emitted in the broad line region by a plasmoid moving out with the jet and scattered back toward the incoming plasmoid by an outer plasma clump acting as a mirror. We consider both a scenario based on a *static* mirror located outside the BLR, and an alternative provided by a *moving* mirror geometry. We show that mirroring phenomena can locally enhance the density and anisotropy with associated relativistic boosting of soft photons within the jet, so as to trigger bright inverse Compton gamma-ray transients from nearly steady optical/X-ray synchrotron emissions. In this picture we interpret the peculiarly asymmetric lightcurves of the recently detected gamma-ray flares from 3C 279. Our scenario provides a promising start to understand the widening class of bright and transient gamma-ray activities in blazars.

Subject headings: gamma rays: observations — FSRQ objects, individual: 3C 279, 3C 454.3

¹INAF/IAPS–Roma, Via del Fosso del Cavaliere 100, I-00133 Roma, Italy

²Univ. “Tor Vergata”, Via della Ricerca Scientifica 1, I-00133 Roma, Italy

³Gran Sasso Science Institute, viale Francesco Crispi 7, I-67100 L’Aquila, Italy

1. Introduction

Blazars are active galactic nuclei (AGNs) whose emissions are dominated by the Doppler boosted radiation from relativistic jets (Urry & Padovani 1995). Blazar radiations - differently from plain Quasars' - are highly non-thermal. They are powered by a central supermassive black hole (BH) that launches the jets closely along our line of sight with considerable bulk Lorentz factors $\Gamma \sim 10$. In the jet, highly relativistic electrons with random Lorentz factors up to $\gamma \sim 10^3$ produce the radiations we observe. These bear a clear non-thermal mark in their spectral energy distribution (SED) that gathers into two main humps, see Fig. 1. An optical-UV peak extending out to soft X rays is commonly understood in terms of synchrotron (S) emission by the relativistic electron population in the jet magnetic field that attains values $B \sim 1\text{ G}$ at $R \sim 3 \cdot 10^{17}\text{ cm}$ from the BH. A second peak in the GeV range is widely discussed in terms of inverse Compton up-scattering by the same electron population of soft ("seed") photons¹ (see, e.g., Sikora, Begelman & Rees, 1994).

The seeds may just comprise the contribution by the very S emission in the jet, the so called synchrotron self-Compton (SSC) process (e.g., Maraschi et al. 1992, Bloom & Marscher 1996). On the other hand, in the external Compton (EC) radiation mode the seeds are dominated by the photons produced in the optical Broad Line Region (BLR) at $R \sim 3 \cdot 10^{17}\text{ cm}$, or by the dusty infrared torus at somewhat larger distances (e.g., Dermer et al. 1992, Sikora et al. 1994). Both regions reprocess/reflect the UV glow of the inner accretion disk around the BH. In fact, the relative heights of the S and of the inverse Compton peaks mark the two basic Blazar flavors: the BL Lac type with comparable heights for which the SSC process may be adequate, and the Compton-dominated (and so gamma-ray dominated) Flat Spectrum Radio Quasars (FSRQs) for which a substantially larger density of seed photons is needed (e.g., Sikora et al. 2009, Boettcher et al. 2013).

Blazars of both flavors have been found to be highly variable, and particularly so in gamma rays. In fact, a new class of gamma-ray Blazars of the FSRQ flavor is now emerging that is marked by flares with extreme properties such as:

1. very large gamma-ray luminosities up to $L_\gamma \sim 10^{48}\text{ erg/s}$ in the range 100 MeV - 10 GeV, together with a large ratio $L_{jet}/L_{disk} \sim 10$;

¹ For standard expressions of the powers and frequencies radiated by the synchrotron and inverse Compton processes we refer the reader to Vittorini et al. 2014, Appendix. In the following, it will be useful to keep in mind that the observed luminosity (for the usual isotropic evaluation) or the corresponding SED follow the proportionality $L \simeq \epsilon F_\epsilon \propto \Gamma^4 U' V'$, in terms of the emitted photon energy ϵ , the energy density of seed photons U' and the emitting volume V' both in the jet comoving frame.

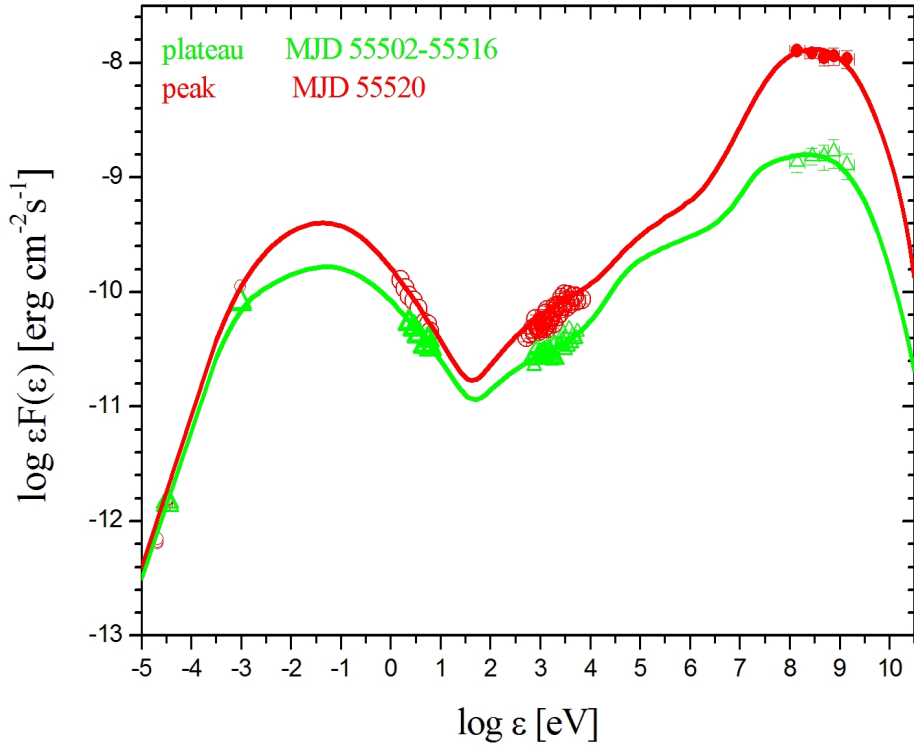


Fig. 1.— The two-humped Spectral Energy Distribution from a FSRQ Blazar with large Compton dominance. Here it is represented the behavior of 3C 454.3 in November 2010, when the Compton dominance was particularly enhanced around the MJD 55520. Details of the spectral fit represented here can be found in V14; in particular, the magnetic field governing the synchrotron emission is $B \simeq 1$ G, and the high-energy electron distribution is modeled as a flat power-law with break energy $\gamma \simeq 10^3$.

2. strong Compton dominance with $L_\gamma \gg L_S$, only marginally correlated in time with optical emissions and even less with soft X rays;
3. short variability time scales, down to a few hours;
4. unusually hard gamma-ray spectra corresponding to SEDs flat or even rising beyond 100 MeV with photon index as hard as 1.6, that in the EC process imply flat electron energy distributions up to a break value $\gamma \sim 3 \cdot 10^3$;
5. occasional spikes at TeV energies.

In addition to 3C 454.3 (e.g., Vittorini et al. 2014) and 3C 279 (Giuliani et al. 2009, Hayashida et al. 2012, 2015) several prominent FSRQs show similar features, at least episodically including PKS 1510-089 (Abdo et al., 2010a, Saito et al., 2013), PKS 1830-211 (Donnarumma et al., 2011), OJ 248 (Carnerero et al., 2015). It is becoming clear that the full behavior of blazar sources is complex and not easily amenable to a single and universal source structure. A widely entertained picture addressing the emissions from FSRQs has been based on the so-called one-zone modeling, with S and EC radiations produced in the *same* region within, or close to the BLR at $R \sim 0.1$ pc (for BLR properties, see Peterson 2006). This constitutes the canonical picture that has to withstand the wealth of incoming new data.

However, such models have been recently shown by Vittorini et al. 2014 (hereafter V14) to fail in accounting for the strong gamma-ray flaring of 3C 454.3. A similar conclusion is implied by Hayashida et al. (2015, hereafter H15) in the case of the 2013-2014 gamma-ray activity of 3C 279. Both sources have clearly shown episodes of *decoupled* gamma-ray and optical/X-ray radiations, with complex and specific timings which include:

- stretches of enhanced, flickering gamma-ray emission spanning weeks or months (that we name "plateau");
- on top of a plateau, day-long gamma-ray flares attain luminosities $L_\gamma \gg L_S$ having little if any counterparts in the optical band and in soft X rays, whilst some optical flashes occur with no corresponding gamma-ray counterpart;
- short time scales down to a few hours, with even faster rise times marking the truly bright flares;
- slow ups and downs occurring in the optical and/or soft X-ray bands on scales of several months to years, with mild maxima and no detailed correspondence with the gamma-ray flares.

Note that episodes of gamma-ray activity including sharp flares often occur near the top of such secular enhancements in the optical or soft X-ray bands. Furthermore, a location of the EC source in an extended environment as rich in UV photons as the BLR would imply a prompt degradation of the spectra at $h\nu > 10$ GeV by photon-photon interactions producing electron - positron pairs. This process would prevent hard spectra from reaching the observer.

Our paper will address these issues and is structured as follows. We will start with a discussion of observed time scales and features of the gamma-ray vs. optical/X-ray radiations, focused on the two prominent FSRQ sources 3C 454.3 and 3C 279. We discuss how the complex correlation patterns in these bands challenge the canonical one-zone structure for the sources. We then summarize the basic idea underlying a viable alternative to one-zone models that we proposed for 3C 454.3 (V14). This is based on a *mirror-driven process* within the jet for inducing localized and transient enhancements of S photon density *beyond* the BLR. The process naturally provides localized seed photon densities large enough for intense and short EC production of gamma rays. We consider separately static and moving-mirror scenarios and carry through our discussion on how they apply to gamma-ray flaring blazars. In particular, we focus on the flares of 3C 279 in 2013-2014 and on their extreme features. We finally discuss how our physical picture is related with dissipation of magnetic energy ultimately producing both the dense photon bath and the acceleration of highly relativistic electrons that concur to feed the EC radiations.

2. The challenge from multiple time scales and missing correlations

As anticipated in Sect. 1 most leptonic models for FSRQs are based on electron S emission prevailing up to the UV and soft X-ray bands, and on inverse Compton radiation taking over beyond. The latter process is fed when the relativistic electrons in the jet up-scatter seed photons provided by internal S emission and/or by external sources like the UV accretion disk and its reprocessed radiations such as the optical lines and the IR torus emissions. The broad-band SED is shaped at any moment by the prevalence of one or the other process.

The one-zone models, in particular, envisage radiations from the *same* region, typically the BLR at distances $R_{BLR} \simeq 3 \cdot 10^{17}$ cm, and so predict neatly *correlated* emissions from the optical to the gamma-ray band over most time scales, as discussed by, e.g., Paggi et al. (2009) for the standard SSC radiation. However, as we show in detail below, such a strong correlation is itself challenged by the data, particularly by several detailed observations of 3C 454.3 and 3C 279. In fact, these FSRQs show a number of *diverse* time scales that

particularly differ from gamma to X rays. For strong gamma-ray flares the risetimes can be as short as 1 hr (limited by the effective instrumental time resolution); on the other hand, the plateaus last up to several weeks. Meanwhile, the X rays show just mild undulations on scales of several months (see Fig. 2). Additional constraints are set by the hard observed spectra that require in and around the source a low optical depth for pair producing photon-photon interactions.

Meeting all such challenges together apparently requires that in different bands not only different source geometries apply, but also different physical processes proceed independently of each other. Our aim is to see whether in fact these can be *related* in a wider physical picture, and connected as tesserae composing a comprehensive pattern.

2.1. The case of 3C 454.3

3C 454.3 in particular features stretches of high-energy activity lasting months/years but also long, inactive states. Since the beginning of systematic gamma-ray observations (and related multifrequency monitoring) in 2007, 3C 454.3 displayed several very intense gamma-ray flaring episodes, notably in November 2009 and 2010 (Vercellone et al. 2010, Striani et al. 2010, Vercellone et al., 2011, Wehrle et al. 2012, Jorstad et al. 2013).

In particular, the November 2010 episode featured for several days the most intense gamma-ray flaring source ever detected, an episode that was notably superimposed on an enhanced plateau emission lasting several weeks. Such sequences (short flares on top of a long plateau) had been previously noted in the EGRET data, a notable example being that of PKS 1622-287 (Mattox et al. 1996). However, EGRET could not follow in detail the lightcurve for extended times, and therefore such a kind of features remained neglected.

On the other hand, AGILE and Fermi by their long pointings provided extended lightcurves, and could test whether the sequence "flare on plateau" constitutes an exception or rather a common mode of strong gamma-ray flaring in FSRQs. In particular, the very intense and complex flare of November 2010 was focused and modelled by V14. In that case, the Compton dominance was enhanced in the flare relative to the plateau – itself up by a factor of 2 – by a further factor of 6.

2.2. The extreme case of 3C 279

3C 279 shows - in a context of flares on top of a plateau - several episodes of enhanced gamma-ray emission with even larger Compton dominance, extended spectral hardness, and

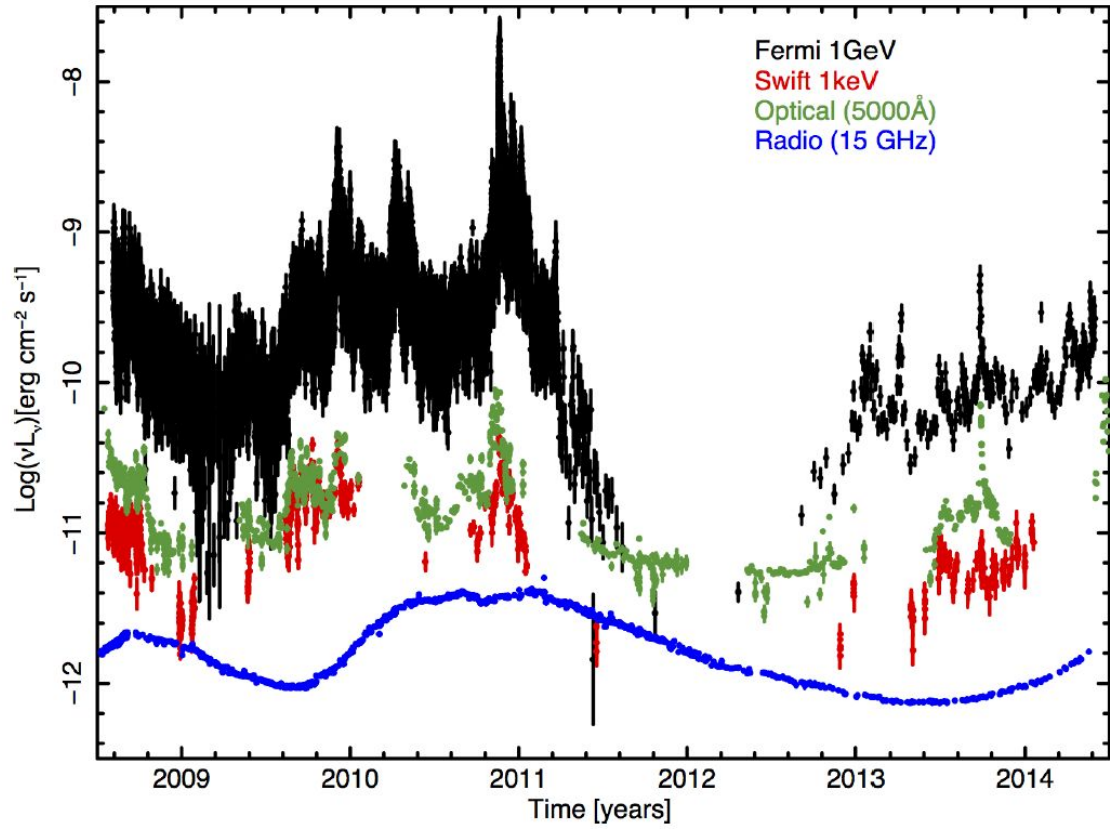


Fig. 2.— Multifrequency monitoring of 3C 454.3 (from Giommi et al. 2015).

lack of optical/X-ray correlations. Since 2007, 3C 279 has been monitored above 100 MeV by AGILE (Giuliani et al. 2009) and Fermi (Abdo et al. 2010b, Hayashida et al. 2012, 2015). Its recent activity during the period 2013-2014 was reported by H15 (see Fig. 3 that we adapt from H15). Their paper includes multi-frequency coverage from the gamma-ray activity lasting several months to the X-ray and the optical (V and R) outputs.

In the context of our previous discussion, three points are particularly relevant:

- 3C 279 is one of the FSRQs detected by Fermi featuring plateau emissions of different intensity levels lasting months/years;
- during the period 2013-2014, this source produced very intense gamma-ray flares (marked by arrows in our Fig. 3, adapted from H15) for which $L_S/L_\gamma \lesssim 10^{-1}$, with no correlated optical or X-ray enhancements;
- flare "1" of H15 and Fig. 3 at MJD 56646 shows a particularly short risetime (~ 1 hr) and a remarkably hard gamma-ray spectrum (photon index ~ 1.6) with no optical counterpart.

Therefore, we have to acknowledge that a number of gamma-ray flares from 3C 279 (as well as those from other extensively monitored FSRQs) do *not* correlate with optical and soft X-ray events of comparable power and time scales. In many cases the former last less and rise more sharply to a much higher Compton dominance, often on top of a much longer and lower plateau; they are observed to cover an extended range of photon energies from 100 MeV to some 10 GeV.

The combination of these features is *beyond* the reach, and even against the predictions, of the canonical one-zone source structure that by construction yields highly correlated S and EC radiations. In addition, to produce intense EC this simple structure requires a dense and extended bath of seed photons that easily could absorb by pair production the high energy radiation after emission. Thus we are led to investigate alternative emission scenarios; we discuss next a "mirror" process, possibly the simplest variant of one-zone modelling.

3. A viable alternative: mirrors

In our approach, a "mirror" is provided by an individual plasma cloud or clump with number density $n \sim 10^6 \text{ cm}^{-3}$ and size $r_m \sim 10^{16} \text{ cm}$ located within the jet opening angle. Such a cloud reprocesses and scatters back part of the impinging S radiation, emulating a

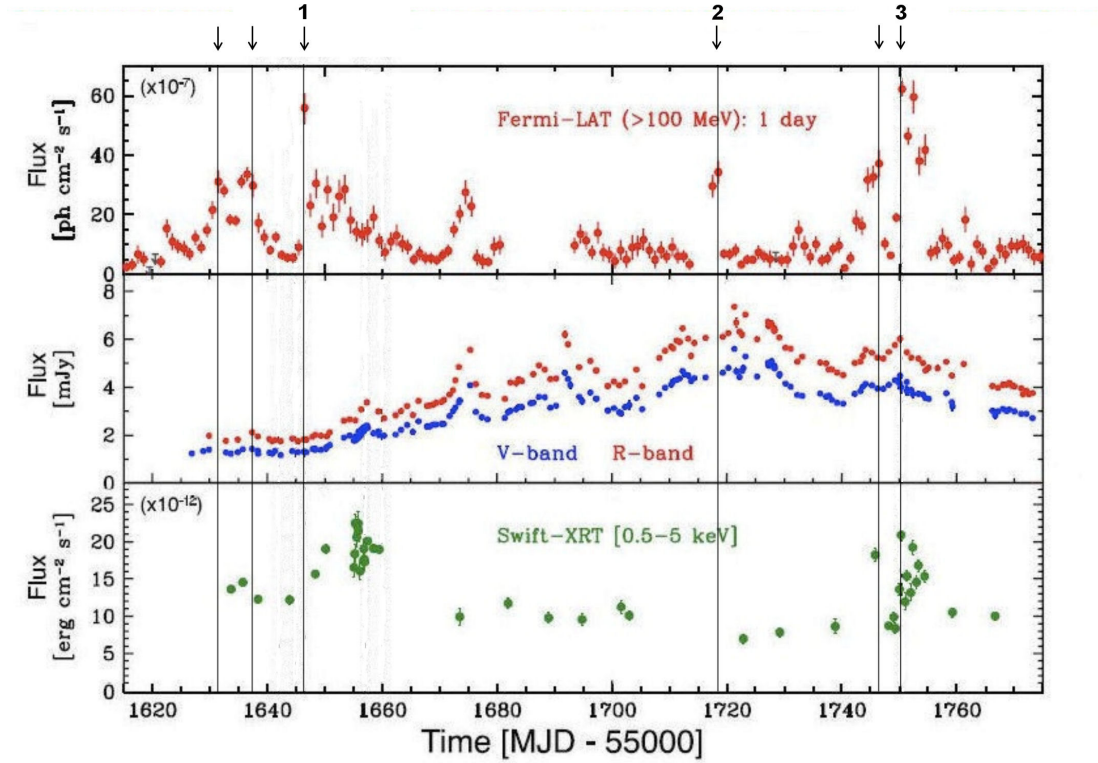


Fig. 3.— Multifrequency monitoring of 3C 279 (adapted from Hayashida et al. 2015). *Top panel:* Fermi-LAT gamma-ray lightcurve above 100 MeV. *Middle panel:* optical data in the R-band. *Lower panel:* Swift X-ray data. The vertical lines highlight the flaring episodes of interest here, i.e., events with little or no simultaneous optical/X-ray emissions. Flares marked as 1, 2 and 3 are labelled in the same way as in H15.

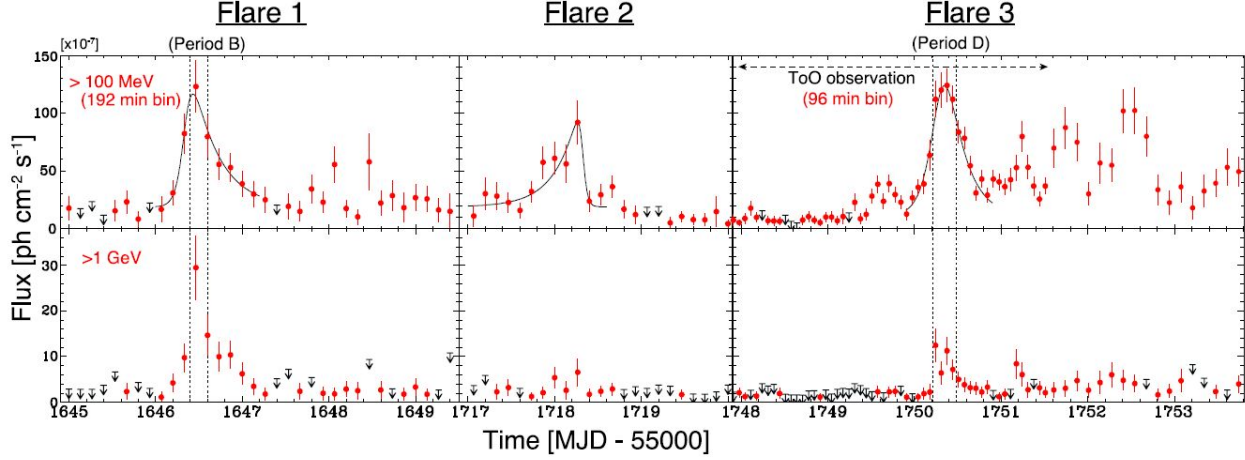


Fig. 4.— Lightcurves observed in flares 1, 2, and 3 of 3C 279 (see Fig. 3) as reported by Hayashida et al. 2015.

”reflectivity” $f \sim 0.1$. Such a value is large enough to provide a relevant enhancement of seed photons before the mirror. Mirrors located within the BLR or near its boundary have been discussed by a number of authors (Madau & Ghisellini 1996, Böttcher & Dermer 1998, Böttcher 2005, V14, Aliu et al. 2014); a location beyond the BLR was recently advocated by V14 who focused on the observations of 3C 454.3.

The action of a mirror *outside* the BLR is indicated by a number of conditions required to explain the observations: strong and fast EC flares from a large but localized density of soft photons; production of gamma-ray flares uncorrelated with comparable emissions in the optical/X-ray bands; flares standing on top of a longer plateau; unabsorbed high-energy spectra. These requirements motivated us to take up the mirror geometry and substantially modify it to operate at distances *beyond* the BLR. At these distances, little gamma-ray absorption is expected from pair production by interactions with surrounding photons so that hard spectra can outgo unscathed.

The geometry adopted by V14 envisaged a *static* mirror similar in size and density to a cloud in the BLR, but located at a larger distance $R \sim 10^{18}$ cm. Our present picture contemplates also moving mirrors, i.e., the reflection and emission resulting from clumps (”plasmoids”) that outflow along the jet with different speeds. The primary emission from a plasmoid within the BLR can be reflected back by a static cloud or by preceding plasmoids acting as mirrors moving on the same track beyond the BLR region. The key feature of our model is constituted by a confining *gap* for reflected seed photons originated

as S emission from plasmoids carrying their share or retinue of relativistic electrons. We will see that the gap constitutes a transient structure marked by a narrow width and by short time scales. Such features break any detailed correlation between the slow variations of the large-scale magnetic field governing the S emission, and the build up of the localized photon density inducing the EC process. We discuss below how such a scenario can meet all of the above requirements.

3.1. A static mirror

In the static mirror case, a partially reflecting cloud is assumed to cross the jet’s radiative cone at a distance R_m from the central BH. The mirror reflects back a fraction $f \sim 10\%$ of the S photons emitted by active plasmoids as they travel with the jet. If the plasmoids share with the jet a bulk Lorentz factor $\Gamma \sim 10$, they will approach the mirror at a relativistic speed $\beta c = c(1 - \Gamma^{-2})^{1/2} \simeq 0.995 c$.

The photons start out from the emitter when this is well below the position of the mirror, at a distance $R_1 \ll R_m$ from the central BH, where the magnetic field is still large enough for intense S emission to occur (see the lower part of Fig. 7). After reflection, photons travel back to meet again the advancing emitter, and are confined to the narrowing gap between it and the mirror (see the upper part of Fig. 7). In simple form, the relativistic travel-time condition for this to occur is given by $R_m - R_1 - d = \beta(R_m - R_1 + d)$, see Böttcher & Dermer (1998) and V14. This leads to evaluate the gap size d in the limiting form

$$d \sim \frac{R_m}{4\Gamma^2} \quad (1)$$

in the laboratory frame. As the plasmoid approaches the mirror, the gap shrinks down to match the mirror size; so, it attains a few times 10^{16} cm, with a related time scale d/c of a few days.

Consider now that the energy density in the gap, as experienced by the advancing emitter plasmoid (with the associated relativistic electrons), is *mirror-boosted* both on the outward and on the inward leg of the photons’ journey. So it reads $U'_m = \eta U_m \Gamma^2$ (see Eqs. B3 and B4 in Appendix B and Appendix C), that is,

$$U'_m = \frac{f \eta}{2 \pi c} \left(\frac{r_m}{R_m} \right)^2 \frac{L'_S \Gamma^4}{d^2} \Gamma^2. \quad (2)$$

Here η is an angular factor of order unity (detailed by Eq. C7 in Appendix C) and $L'_S \sim 10^{42} \text{ erg s}^{-1}$ is the co-moving S luminosity from a plasmoid near R_1 , corresponding in

the usual isotropic evaluation to an observed value $L_S = L'_S \Gamma^4 \sim 10^{46}$ erg/s. Note that the process of mirror-boosting introduces the additional factor $\eta \Gamma^2$ in the expression for the comoving energy density U'_m . Indeed, Eq. 2 shows that U'_m has a dependence on Γ that results from the energy density as seen by the mirror (the factor Γ^4), times a further factor $\eta \Gamma^2$ induced by mirror reflection.

The photon energy density in the gap as given by Eq. (2) induces a flare of up-scattered EC gamma-ray emission that grows as $1/d(t)^2$ to yield a sharp spike. The specific time decrease of $d(t)$ is given by Eq. A11 in Appendix A, and the resulting rise of the flare is represented in Fig. 5.. Eventually, $d(t)$ narrows down to match the mirror size r_m and the gamma-ray intensity attains its peak. Using the travel-time condition (Eq. 1) to expose the overall dependence on Γ , we obtain the peak value

$$U'_{m,p} = \frac{16 f \eta}{2 \pi c} \left(\frac{r_m}{R_m} \right)^2 \frac{L_S}{R_m^2} \Gamma^6. \quad (3)$$

Note that similar high powers of Γ also arise in similarly anisotropic conditions implying head-on photon-electron collisions as discussed e.g., by Dermer & Schlickeiser 2002, Sikora et al. 2009, Ghisellini & Tavecchio 2009.

From Eq. 1, the timescale for the lightcurve rise in the observer's frame turns out to be

$$T \simeq \frac{R_m}{4 c \Gamma^4}, \quad (4)$$

that is, a few hours. After having reached its peak, the lightcurve may fall abruptly if the seed photon replenishment is cut off. Such a condition occurs when plasmoid and mirror merge (as the approaching plasmoid screens out the mirror from the incoming photons), and/or when the plasmoid sidesteps the mirror and relativistic de-boosting applies. Such conditions occur on an observer's timescale of order $\sim r_m/2 c \Gamma^2 \sim 1.5$ hr, and may yield strongly asymmetric flares as observed in 3C 279 (flare 2 of Figs. 4 and 5).

As to the gamma-ray luminosity L'_γ , one has to account also for the emitting volume with its possible dependence on Γ . In fact, if the volume comprises just the plasmoid and its close vicinity, it will not depend on Γ and the scaling of L'_γ will be $L'_\gamma \propto \Gamma^6/R_m^2$, as given by the limiting Eq. 3. On the other hand, if the emitting volume involves the whole gap and reads $\pi r_m^2 d'$ (where $d' = d/\Gamma$ is the comoving gap width), it will start from large values and eventually shrink to $\pi r_m^3/\Gamma$, so that $L'_\gamma \propto \Gamma^5$ holds. In either case, the interesting possibility arises of bright and short gamma-ray flares induced *outside* the BLR.

It is also important to check in the plasmoid frame the source opacity, $\tau'_{\gamma\gamma} \sim n'_{ph} (\sigma_T/3) l'$ due to pair production by photon-photon interactions; here σ_T is the Thomson cross section, and l' a typical integration length. Pair production against the observed GeV photons

occurs for comoving photon energies $(1 \text{ GeV})/\Gamma$ against softer photons of energies $\epsilon' \simeq 10 \text{ keV}$, that are reflected by the mirror at energies $\epsilon \simeq 1 \text{ keV}$. Denoting by $\alpha_{\text{keV}} \lesssim 10^{-1}$ the fraction of mirror-reflected luminosity in the latter range, we have

$$\tau'_{\gamma\gamma} = \frac{f \eta \sigma_T \alpha_{\text{keV}}}{6 \pi c \epsilon'} \left(\frac{r_m}{R_m} \right)^2 l' \frac{L_S}{d^2} \Gamma^2 = \frac{f \eta \sigma_T \alpha_{\text{keV}}}{6 \pi c \epsilon'} \left(\frac{r_m}{R_m} \right)^2 l' \frac{L_S}{d'^2} \quad (5)$$

where in the last expression we have used again $d' = d/\Gamma$. Over a comoving integration path $l' = d'$, we have

$$\tau'_{\gamma\gamma} = \frac{f \eta \sigma_T \alpha_{\text{keV}}}{6 \pi c \epsilon'} \left(\frac{r_m}{R_m} \right)^2 \frac{L_S}{d'} \simeq 2 \cdot 10^{-4} \frac{L_{S,46}}{R_{m,18}} \frac{\alpha_{\text{keV}}}{0.1} \Gamma^3, \quad (6)$$

where we adopted $r_m/R_m = 1/30$, $L_{S,46} = L_S/(10^{46} \text{ erg s}^{-1})$, and $R_{m,18} = R_m/(10^{18} \text{ cm})$. For $\Gamma \sim 10$, in the gap we find $\tau'_{\gamma\gamma} \lesssim 1$. Whence we obtain the upper limit for the static mirror distance $R_m \simeq 5 \cdot 10^{17} \text{ cm}$ within which pair absorption is significant. For larger distances, the optical depth for pair production is less than unity.

Such a mirror geometry can explain in simple terms the puzzling behavior of 3C 454.3 in November 2010, and also that of 3C 279 at the peak of the lightcurve marked as "flare 2" by H15 (see our Fig. 3), including the absence of comparable correlated enhancements of the S emission in the optical band and the hard spectra observed to escape from the source.

A static mirror of reflectivity $f \sim 10\%$ may be provided by a stray BLR cloud hit by the jet (V14), or by the atmosphere of a red giant star crossing the jet (Khargulyan et al., 2013), or more likely by a lagging plasmoid left over in the jet by a previous ejection episode. We favor the latter possibility since it makes easier for a plasmoid to pick up a suitable mirror, and also because the observed flickering plateau apparently requires - in addition to the large emitter plasmoid originating the strong spike - a whole string (a "train" in the terminology of V14) comprising many smaller companions.

3.2. A moving mirror

The moving-mirror scenario envisages successive plasmoids formed and ejected along the jet at different times with different speeds. A plasmoid moving outwards at a velocity $c\beta$ as discussed in the previous subsection may find on its track another, lagging member of a string previously ejected, cruising at a slower speed $c\beta_o < c\beta$. Then the back side of the preceding plasmoid can provide a moving mirror for the following one. This condition is analyzed in detail in the Appendix A, and the main results are reported here (see Fig. 7 for details and definitions). For simplicity, we focus here on the representative case of constant speeds, and postpone the case of time variable speeds to a forthcoming publication.

Recall first that in a static mirror geometry the photons emitted at position z_1 and time t_1 propagate outwards over a distance x_1 to a mirror position \tilde{R}_m ; then they are reflected back to meet the emitter after propagating over an additional distance x_2 . Meeting at the point z_2 is governed by the travel-time condition that rewrites as $z_2 - z_1 = \beta(x_1 + x_2)$ after Böttcher & Dermer (1998), where we used the shorthands: $z_1 = R_1$, $z_2 = \tilde{R}_m - \tilde{d}$, and the definitions $x_1 = \tilde{R}_m - R_1$, $x_2 = \tilde{d}$ (see Appendix A and Fig. 7). In the case of a moving mirror, we have to consider also the speed β_o of the mirror itself, in addition to the speed β of the plasmoid emitting the primary S radiation.

Here it is convenient to define the confining *gap* as the distance \tilde{d} between the mirror location $Z(t_r)$ at the reflection and the position $z_2(t_C)$ reached by the plasmoid at the time t_C of the Compton radiation (which provides the abscissa t of the representative gamma-ray lightcurve plotted in Fig. 5); this yields $\tilde{d} = Z(t_r) - z(t_C)$ which is calculated (see Eq. A18) to read

$$\tilde{d} = D_{in} \left[\frac{(1 - \beta)}{(1 + \beta)(1 - \beta_o)} \right]. \quad (7)$$

Here the quantity $D_{in} = \Delta z + \beta_o c(t_1 - t_o) \equiv \Delta z + D_o$ is the sum of two components: (1) an initial distance $\Delta z = \tilde{R}_m(t_1) - R_1(t_1)$ between the moving mirror at radius \tilde{R}_m and the point R_1 where the emitter radiates; (2) a kinematic mirror-plasmoid initial distance $D_o = \beta_o c(t_1 - t_o)$ travelled by the mirror during the time interval $t_1 - t_o$.

Eq. 7 constitutes our main *kinematic* result for the case of a moving mirror. For a static mirror with $\beta_o = 0$ it goes into Eq. 1; on the other hand, for $0 < \beta_o < \beta$ the distance \tilde{d} may be approximated as

$$\tilde{d} \simeq \frac{D_{in}}{2} \left(\frac{\Gamma_o}{\Gamma} \right)^2. \quad (8)$$

Thus the distance between the mirror advancing at a speed $\beta_o c$ and the plasmoid catching up with a speed βc can be made substantially shorter than D_{in} , at the time of the inverse Compton up-scattering of the reflected photons. In terms of the *relative* Lorentz factor $\Gamma_r \simeq \Gamma/2\Gamma_o$ (the simple expression that holds for $\Gamma_o^2 \gg 1$, $\Gamma^2 \gg 1$, and $\Gamma > \Gamma_o$, see Appendix C) Eq. 8 writes in the form $\tilde{d} \simeq (D_o/2)/(4\Gamma_r^2)$ analogous to Eq. 1.

The energy density (in the plasmoid comoving frame) of the reflected photons that trigger Compton scattering writes as (see Eq. B11, and Appendix C for details)

$$U'_m = \tilde{\eta} U_m \Gamma_r^2 = \frac{f \tilde{\eta} L'_S}{2\pi c} \left(\frac{r_m}{D_o} \right)^2 \frac{1}{D_o^2} \left(\frac{\Gamma}{\Gamma_o} \right)^8 \Gamma_r^2, \quad (9)$$

where Γ_r is the Lorentz factor of the plasmoid *relative* to the moving mirror, and Eq. 8 has been used for the gap size for $\Delta z = 0$. In Eq. 9 we denoted with L'_S the S luminosity emitted

at the height z_1 by the plasmoid in its comoving frame. Values that reasonably apply to a moving mirror-plasmoid configuration of interest here are $r_m \simeq 3 \cdot 10^{16}$ cm, $D_o \simeq 3 r_m$, $f = 0.1 f_{-1}$, and $\Gamma_o = 3$. Thus we have the limiting value

$$U'_m \simeq (f_{-1} 10^{-7} \text{ erg cm}^{-2}) L'_{42} \frac{1}{(\Gamma_o/3)^2} \left(\frac{\Gamma}{\Gamma_o} \right)^8 \Gamma^2, \quad (10)$$

where $L'_{42} = L'_S/(10^{42} \text{ erg s}^{-1})$.

For a given number of energetic electrons, it is useful to refer to a typical photon energy density around a plasmoid moving through the photon bath of the BLR, that reads

$$U'_{BLR} = \frac{4}{3} \frac{\xi_{BLR} L_D \Gamma^2}{4 \pi c R_{BLR}^2} \simeq (0.03 \text{ erg cm}^{-3}) L_{D,46} \frac{\xi_{BLR}}{0.1} \Gamma^2. \quad (11)$$

Here we used the disk luminosity $L_{D,46} = L_D/(10^{46} \text{ erg s}^{-1})$, the radius $R_{BLR} = 3 \cdot 10^{17}$ cm, and the average BLR covering factor $\xi_{BLR} = 0.1$. The value of U'_{BLR} rapidly decreases outside the BLR, and there would be little seed photon density available for inverse Compton scattering, were it not for the mirror mechanism. Outside the BLR, U'_m can exceed the value U'_{BLR} previously encountered in the BLR for a range of plasmoid kinematic and radiative conditions; so the effectiveness of a mirror in producing gamma-ray flares can vary. An interesting situation arises when U'_m is comparable to, or larger than the BLR value. In fact, $U'_m \geq U'_{BLR}$ obtains for

$$\frac{\Gamma}{\Gamma_o} \gtrsim 4. \quad (12)$$

Accordingly, an interesting configuration for the moving mirror-plasmoid geometry is obtained with the following parameters: $\Gamma \simeq 10 - 15$, $\Gamma_o \simeq 2 - 3$, $r_m \simeq 3 \cdot 10^{16}$ cm, and a location beyond the BLR radius.

Thus a moving mirror geometry can provide conditions *internal* to the jet for a substantial enhancement of the local photon bath at a considerable distance from the BLR. In fact, in this geometry the distance where the EC radiation can occur and constitute a strong gamma-ray flare with (isotropized) $L_\gamma \sim 10^{46} \text{ erg s}^{-1}$ is

$$\delta z = z_2 - z_1 = 2 \beta D_{in}/(1 + \beta)(1 - \beta_o) \simeq 2 D_{in} \Gamma_o^2, \quad (13)$$

which can substantially exceed R_{BLR} . For reference values $D_o \simeq 3 r_m$, $r_m \simeq 3 \cdot 10^{16}$ cm and with $\Gamma_o = 2$, we have

$$\delta z \simeq 7 \cdot 10^{17} \text{ cm}, \quad (14)$$

while for $\Gamma_o = 4$ we have

$$\delta z \simeq 3 \cdot 10^{18} \text{ cm}. \quad (15)$$

An effective mirror mechanism for gamma-ray production can therefore operate just outside the BLR boundary or somewhat beyond, depending on jet conditions. On the other hand, an upper limit $z_1 < 0.3$ pc to the distance within which the plasmoid efficiently radiates by EC is set by the condition that below the mirror the magnetic field be high enough to produce a primary, comoving S radiation $L'_S \gtrsim 10^{42}$ erg/s to illuminate the mirror.

To summarize: plasmoids of sizes $r_m \sim 3 \cdot 10^{16}$ cm with somewhat wider spacings (condensed by a jet instability to form a string of a few dozens) can emit, partially reflect and transiently confine S photons to produce intense and short Compton flashes. The primary power L'_S can be fed as the emitter sweeps the surrounding average magnetic energy at a rate $\pi r_m^2 \beta c B^2 / 8\pi \sim 10^{42} B^2$ erg/s (with B in Gauss), provided that such a power goes into replenishing the electron energies up to values $\gamma \gtrsim 10^3$. A fitting physical process to embed both a prolonged electron acceleration and the fragmentation/coalescence process of jet plasma into plasmoid strings is suggested on noting that fast gamma-ray flares often arise near the maxima of mild, slow enhancements of S emission in the optical - soft X-ray bands (see Fig. 2 for the case of 3C 454.3). In other words, mild large-scale growth of the magnetic field apparently paves the way to bright small-scale activity at high energies.

Such conditions match those expected from a scenario of magnetic reconnections in a collisionless plasma (see Kagan et al. 2015, who review classic theoretical work and their own recent numerical simulations); the process is started where large-scale field reconfigurations in the jet set layers of opposite, annihilating \mathbf{B} lines. The magnetic energy so liberated feeds kinetic tearing instabilities that lead to local jet *fragmentation* into strings of separate plasmoids. These include a few giant ones arising from repeated cycles of coalescence and condensation of smaller companions. The cycles are to take the fragments from the minimal, kinetic scales set by the inertial skin depth at $10^2 c/\omega_p$ in terms of the electron plasma frequency $\omega_p \simeq (5 \cdot 10^4 \text{ s}^{-1})(n/\gamma)^{1/2}$ (where n is the electron number density in units of cm^{-3}), up to the sheath overall length $2\ell \sim$ several light-days (see Fig. 7).

Meanwhile, the ensuing electric fields efficiently *accelerate* electrons up to energies $\gamma \gtrsim 10^3$ in, or between the plasmoids even under initial conditions of moderate magnetization $\sigma = B^2/\Gamma n m_p c^2 \sim 10$. Losses by S cooling and by adiabatic expansion are replenished by continuous acceleration going on as long as the process of repeated fragmentation and coalescence lasts in the magnetic reconnection sheaths. Alternatively, magnetic reconnection has been considered in the context of forming mini-jets (e.g., Kagan et al. 2015). However, Narayan & Piran 2012 discuss the considerable relative Lorentz factors of the mini-jets and their large multiplicity, which concur to require a quite large power from the central source.

4. Specific marks of a new class among the gamma-ray flares of 3C 279

We have discussed why in the framework of the canonical one-zone model a S - EC source located in the BLR can account neither for luminosity ratios $L_\gamma/L_S \gg 1$ nor for the lack of detailed correlations between the gamma-ray flares and the synchrotron optical and soft X ray components. It is clear today that a number of gamma-ray flaring episodes from prominent FSRQs show features that are challenging such a framework. Although a comprehensive study and interpretation of all types of gamma-ray flares is beyond the scope of the present paper, we will briefly place our alternative mirror model in the context of the 2013-2014 activity of 3C 279 that provides a collection of diverse flare prototypes.

We based our considerations on the recent observations of 3C 279 by H15; in our Fig. 3 we highlight from that paper a number of gamma-ray episodes relevant to our analysis. The vertical lines mark several gamma-ray flares with little or no simultaneous optical and X-ray enhancements. H15 identified three particular gamma-ray flares of interest; we singled out in our Fig. 4 the lightcurves of these events in the range from 0.5 to 10 GeV.

We first focused on "flare 2" that features a markedly *asymmetric* lightcurve. Here the rise over ~ 1 day is followed by a peculiarly sharp fall in less than one hour. This behavior was noted by H15, who parametrized the rise-time and the decay time at 6.4 hr and 0.6 hr, respectively. Such a peculiar shape is not often observed in high-energy sources, and points to a specifically time-asymmetric emission mechanism. We identified such a behavior with that expected from Compton up-scattering of radiation reflected by a moving mirror, as we have computed and shown in our Fig. 5.

From our kinematics we obtained steeply rising spikes from EC triggered by a doubly *boosted* photon density; this is emitted at about the height of the BLR, and then reflected back into the gap between the outer mirror and the advancing plasmoid (see Eq. 10 with its strong dependence on Γ). Eventually, as the plasmoid pastes on, or sidesteps the mirror, the seed photon density decays sharply as the mirror-boosting no longer applies. Fig. 5 shows the sharply asymmetric pattern expected for the lightcurve produced by a mirror process with the simplest kinematic plasmoid-mirror relationship as discussed in Sect. 3. Such a *kinematically* triggered and quenched radiation pulse agrees with the observations of "flare 2" in 3C 279 reported by H15. The detailed agreement between flare 2 and the asymmetric gamma-ray lightcurve produced by our simple mirror mechanism is shown in Fig. 5.

On the other hand, more complex conditions may arise from interactions between mirror and plasmoid as the two get close to near contact, that is, to a distance smaller than r_m . For one, when we also account for mirror motion outwards, Eq. 10 shows that the spike is softened to a more rounded peak as the gap shrinks to the mirror size, and ends into a

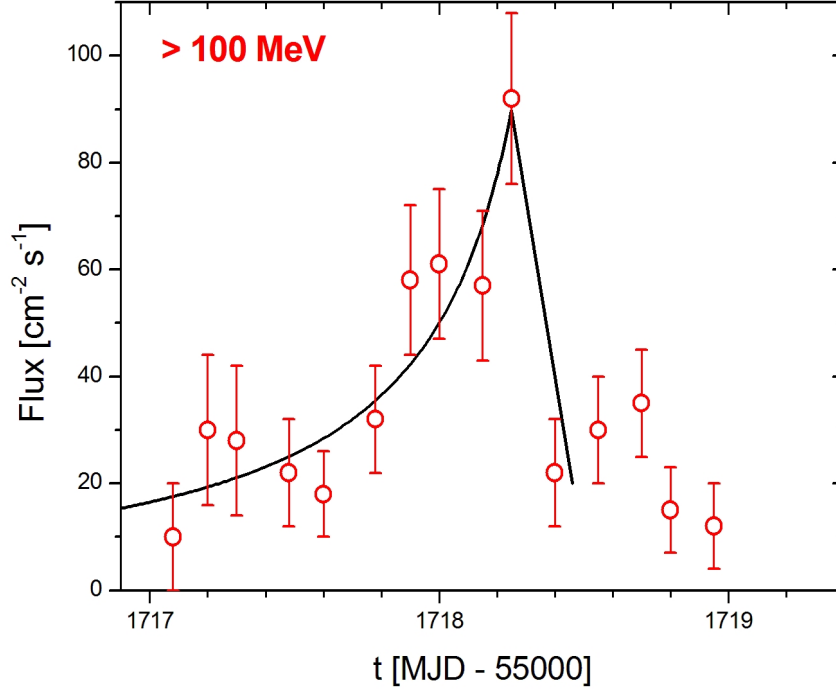


Fig. 5.— Gamma-ray lightcurve of flare 2 of 3C 279 (data points from Hayashida et al. 2015, zoomed from Fig. 4) superimposed to the gamma-ray emission calculated from the mirror-driven mechanism discussed in the text (solid curve). The rise is produced by the seed photon density increasing as $U'_m \propto 1/d^2$ (see Eq. 2) with the gap size $d(t)$ shrinking after the linear relation given by Eq. A11. The sharp fall follows from the sudden decrease of the seed photon density when the emitter crosses or sidesteps the mirror on a timescale shorter than the data resolution (193 min., H15); see Sect. 3.1 for discussion.

stretched decay. In addition, bright EC radiation implies severe electron cooling, while forced electron re-acceleration may occur by compression into the gap of magnetic field lines dragged along by the approaching plasmoid in a delicate balance that is worth discussion. The cooling time of the energetic electrons that emit gamma-ray photons up to GeV energies is to be contrasted with the variability time scale. The inverse Compton cooling time in the comoving frame is given by $\tau'_c \simeq 3 m_e c / 4 \sigma_T U'_m \gamma \simeq (1.5 \cdot 10^4 \text{ s}) \gamma_3^{-1} \Gamma_1^{-2}$, where $\gamma_3 = \gamma / 10^3$, $\Gamma_1 = \Gamma / 10$, and we used as a reference the energy density of the broad line region (Eq. 11 with $\Gamma = 10$). Thus the cooling time turns out to be shorter than the kinematical time $\tilde{d} / \Gamma c \simeq 10^5 \text{ s}$ in the comoving frame. Therefore, the softer decrease of other observed gamma-ray lightcurves has to depend mainly on other factors such as the gap collapse.

In particular, the slow decays of flares 1 and 3 as reported in our Figs. 3 and 4 cannot be accounted for in terms of the associated fast radiative cooling just discussed². Such slow decays point rather to the stretching of the lightcurve over times of days that we expect (as pointed out above) from substantial mirror motion. This is likely assisted by electron re-acceleration as indicated by the particularly hard spectrum of flare 1, see also the recent detection of photon emission above $\sim 50 \text{ GeV}$ from 3C 279 (Paliya, 2015).

In addition to flares 1, 2, and 3, Fig. 3 shows other gamma-ray flaring episodes that do correlate with other bands, and so are amenable to standard interpretations in terms of one-zone source geometry at BLR distance. 3C 279 is also known for its remarkable gamma-ray flare on February 2009 observed to correlate with large swings of optical polarization that may be interpreted in terms of smooth bending of magnetic field lines at parsec distances (Abdo et al. 2010b, see also Zhang et al., 2015). at equal observability/flux. We have in preparation a detailed discussion of diverse kinds of gamma-ray flares between these two extremes. As anticipated in the Introduction, we expect flares belonging to the class discussed here to occur in a number of FSRQs including 3C 454.3, PKS 1510-089, PKS 1830-211, OJ 248.

To summarize: in our approach the *rise* of a number of gamma-ray flares is dominated by localized kinematic effects, i.e., the shrinking photon gap. On the other hand, the *fall* phase may be modulated by other processes. Flare 2 can be interpreted in terms of a purely kinematical event with a decay governed just by gap collapse. Instead, flare 1 and flare 3 show a smoother decay phase, with a particularly hard spectrum in flare 1, providing evidence of particle re-acceleration at work.

²See also Paliya et al. 2015 for a recent discussion of flare-3.

5. Discussion and Conclusions

Strong, sharp flares in gamma rays around 1 GeV are observed in beamed blazars of the FSRQ flavor. These sources are marked not only by a jet-like powerful plasma outflow with a moderate bulk Lorentz factor $\Gamma \sim 10$, but also by SEDs dominated by inverse Compton radiation even in their low states of emission. We have discussed here how and why bright gamma-ray flares *often* do not show clear time correlation with emissions in other bands, while they attain high luminosities so as to increase the Compton dominance by factors up to 10.

Such flares are widely discussed in terms of the external Compton radiation process (i.e., inverse Compton up-scattering of soft “seed” photons), while the emissions from the optical to the soft X-ray band are well understood as synchrotron radiation in the large scale, slowly changing magnetic field $B \sim 1$ G that threads the jet at distance around 0.1 pc from the central BH. Both radiation components are produced by similar or even coinciding populations of ultra-relativistic electrons with break energies $\gamma \sim 10^3$ that inhabit the source. However, a S - EC source with the canonical one-zone geometry cannot account for instances with luminosity ratios $L_\gamma/L_S \gtrsim 10$ and lack of specific correlations between the synchrotron optical and the inverse Compton gamma-ray components.

We found instead that a mirror-like geometry at distances of about 0.3 pc from the central BH can yield the *high* but *localized* and *transient* densities of anisotropic S photons needed for a strong, sharp and short EC flash to occur. This scenario can explain the large observed gamma-ray luminosity, short time scales, and related lack of correlations with the larger scale S emissions. Our geometry is based on S radiation emitted by individual plasmoids at lower heights 0.1 pc in a string outflowing with the jet. Such emission is reprocessed/scattered back by an outer mirror at some $R \sim 0.3 - 1$ pc provided by a large, slow plasmoid in a previous string.

A key feature is constituted by a narrow and shrinking *gap* between the mirror and the approaching plasmoid, where the density of photons is enhanced sharply by double *mirror-boosting* on their outward and inward course. So during time intervals of hours, the photon density attains levels high enough to trigger strong flashes of high-energy IC radiation. Eventually, this emission is saturated and ultimately quenched as plasmoid and mirror come closer than the mirror radius. We emphasize that in this process the Compton dominance is even enhanced relative to the already large value marking the FSRQs in their plateau states. Our gamma-ray lightcurves feature a steep rise, and an even sharper fall when the plasmoid piles up onto, or sidesteps the mirror, so as to suddenly decrease the seed photon density. On the other hand, the process allows hard spectra in the range 100 MeV - 10 GeV to escape from the source, since in and around the narrow gap a low optical

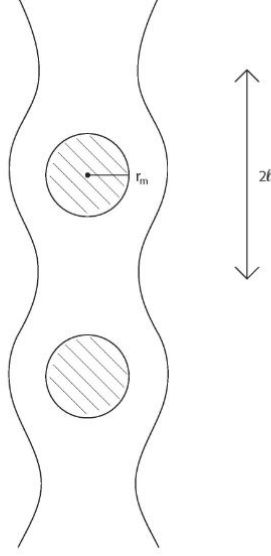


Fig. 6.— Schematic view along the jet z -axis of the flow instability leading to plasmoid formation (see also Kagan et al. 2015).

depth for pair creation by photon-photon interactions applies.

Our specific source model requires active, emitting plasmoids with bulk Lorentz factors $\Gamma \gtrsim 10$ to satisfy the opacity and luminosity requirements; it requires also passive, mirror plasmoids with $\Gamma_o \sim 3$ to locate the flash of EC radiation at the outer edge of the BLR. We name the geometry and emission mechanism discussed in this paper the “Mirrored-Synchro-Compton” (MSC) scenario for gamma-ray production in blazars. The MSC mechanism is marked by strong Compton dominance with no optical/X-ray simultaneous emission during the gamma-ray flares, by asymmetric flare lightcurves, and by short timescales.

Our MSC source geometry fits in with the prevailing physical view that contemplates in the jet a collisionless plasma threaded by large scale magnetic fields that include sheath-like structures; here opposite \mathbf{B} lines run sufficiently close over a distance $2\ell \sim 0.1$ pc to annihilate and convert the magnetic energy into two forms. First, at scales of some 10^2 inertial skin depths indicated by the current numerical simulations (see Kagan et al. 2015) these plasma/field structures become unstable to tearing instability, and *fragment* into strings of many separate condensations, i.e., plasmoids, some of which coalesce into a few giant ones. Thus the macroscopic structure goes through many cycles of instability-

coalescence, with scales up to the sheath overall length of some 0.05 pc (see Fig. 6). Second, at the particle level the electric fields associated with annihilating \mathbf{B} are very efficient in continuously accelerating electrons within and between plasmoids, to attain high random Lorentz factors with energies $\gamma \gtrsim 10^3$. Ultimately, most of the large radiative powers observed in such events is driven by the overwhelming bulk energy flow carried by the jet (e.g., Celotti & Ghisellini 2008).

In conclusion, the radiative and kinematical processes proposed here can provide the building blocks for *intense and fast* gamma-ray flares *uncorrelated* with optical - soft X-rays events that are most difficult to explain in the context of the canonical one-zone geometry. This is achieved by locating the gamma-ray source outside the broad line region; our proposal accounts for the observed features marking of a number of flares: conspicuous increase of Compton dominance; lack of time correlation between gamma-rays and optical/X-ray emissions, hard spectra produced by re-acceleration and not cut off by pair production.

We find the MSC picture discussed throughout the present paper particularly attractive since it offers three relevant features: it makes easier for a plasmoid to find a mirror within the jet; large optical/UV photon densities can be localized just *outside* the broad line region so as to induce *strong* gamma-ray flares in optically thin environments with *no* or *negligible* correlation with other bands; short timescales can be naturally produced. The mirror scenario for transient gamma-ray production presented here can have broad relevance in blazar research.

Acknowledgments: We are indebted to P. Giommi for helpful discussions and for providing Fig. 2. We thank our anonymous referee for useful comments and suggestions. Investigation carried out with partial support by the ASI grants no. I/028/12/0 and I/028/12/2.

REFERENCES

- Abdo, A. et al. 2010a, *ApJ*, 721, 1425
- Abdo, A. et al. 2010b, *Nature*, 463, 919
- Aliu, E., et al. 2014, *ApJ*, 797, 89
- Bloom, S.D. & Marscher, A.P., 1996, *ApJ*, 461, 657
- Böttcher, M. & Dermer, C.D. 1998, *ApJL*, 501, L51
- Böttcher, M., Reimer, A., Sweeney, K., & Prakash, A., 2013, *ApJ*, 768, 54
- Carnerero, M.I. et al., 2015, *MNRAS*, 450, 2677
- Celotti, A., & Ghisellini, G., 2008, *MNRAS*, 385, 283
- Dermer, C.D., Schlickeiser, R. & Mastichiadis, A., 1992, *A&A*, 256, L27
- Dermer, C.D. & Schlickeiser, R. 1994, *ApJS*, 90, 94
- Dermer, C.D. & Schlickeiser, R. 2002, *ApJ*, 575, 667
- Donnarumma, I. et al., 2011, *ApJL*, 736, L30
- Ghisellini, G. & Madau, P., 1996, *MNRAS*, 280, 67
- Ghisellini, G. & Tavecchio, F., 2009, *MNRAS*, 397, 985
- Giommi P., et al., 2015, *arXiv:1503.04863v2*
- Giuliani, A. et al., 2009, *A&A*, 494, 509
- Hayashida M., et al., 2012, *ApJ*, 754, 114
- Hayashida M., et al., 2015, *ApJ*, in press, *arXiv:1502.04699 (H15)*
- Kagan, D., Sironi, L., Cerutti, B. & Giannos, D., 2015, *Space Sci. Rev.*, *arXiv:1412.2451*
- Jorstad, S.G., et al. 2013, *ApJ*, 773, 147
- Khangulyan, D.V., Barkov, M.V., Bosch-Ramon, V., Aharonian, F.A., Dorodnitsyn, A.V. 2013, *ApJ*, 774, 113
- Maraschi L., Ghisellini, G. & Celotti, A., 1992, *ApJ*, 397, L5

- Marscher, A.P. 2014, ApJ, 780, 87
- Mattox, J.R., et al., 1997, ApJ, 476, 692
- Paggi, A. et al. 2009, A&A, 504, 821
- Paliya, V.S., Sahayanathan, S., Stalin, C.S., 2015, ApJ, 803, 15
- Paliya, V.S., 2015, ApJ, 808, 48
- Peterson, B.M. 2006, The Broad-Line Region in Active Galactic Nuclei, Lect. Notes Phys. 693, 77 (Springer)
- Sikora, M., Begelman, M. C., Rees, M. J. 1994, ApJ 421, 153
- Sikora M., Stawarz, L., Moderski, R., Nalewajko, K. & Madejski, G.M., 2009, ApJ, 704, 38
- Saito, S., Stawarz, L., Tanaka, Y.T., et al, 2013, ApJ, 766, L11
- Striani, E. et al. 2010, ATel n. 3034 & ATel n. 3043
- Urry C.M. & Padovani, P., 1995, PASP, 107, 803
- Vercellone, S. et al. 2010, ApJ, 718, 455
- Vercellone, S. et al. 2011, ApJL, 736, L38
- Vittorini, V., Tavani, M., Cavaliere, A., Striani, E., Vercellone, S., 2014, ApJ, 793, 98 (V14)
- Wehrle, A.E. et al. 2012, ApJ, 758, 72
- Zhang, H., et al., 2015, ApJ, 804, 58

A. Appendix: Mirror Kinematics

Let us consider in some detail a geometry in which plasmoid outflow occurs along the z axis perpendicular to the accretion disk plane. Fig. 7 shows the geometry and the meaning of the relevant quantities. Let z_1 and z_2 be two successive positions of a moving plasmoid with velocity βc . Photons emitted at position z_1 and time t_1 propagate through a distance x_1 to a given mirror position, and then are reflected back into the same plasmoid after propagating an additional distance x_2 ; their encounter with the plasmoid at z_2 is governed by the light travel-time condition

$$z_2 - z_1 = \beta (x_1 + x_2). \quad (\text{A1})$$

Eq. A1 applies to a static mirror (Boettcher & Dermer 1998) where we used the definitions given at the beginning of Sect. 3.2. We aim at extending the condition to a moving mirror, i.e., to the case of radiation reflected back by a plasma clump moving in front of the active plasmoid. In such a case two speeds are to be considered: β_o for the reflecting clump, and β for the emitting plasmoid.

We focus on a moving mirror constituted by another plasmoid able to reflect a relevant amount of impinging radiation. We also assume that within the distance span of interest β_o and β are closely constant. Let us consider quantities in the observer's frame. The moving mirror is ejected at the distance z_1^* at time t_o , and moves outward as

$$Z(t) = z_1^* + \beta_o c (t - t_o). \quad (\text{A2})$$

The emitting plasmoid reaches the distance z_1 at time t_1 (with t_1 larger than t_o), and moves outward according to

$$z(t) = z_1 + \beta c (t - t_1). \quad (\text{A3})$$

In the following, we define

$$\Delta z = z_1^* - z_1 \quad (\text{A4})$$

In general $\Delta z \neq 0$, but also $\Delta z = 0$ is viable (see below for a physical interpretation). Photons emitted at the position z_1 at time t_1 propagate freely according to $\zeta(t) = z_1 + c(t - t_1)$. Reflection occurs at time t_r under the condition $\zeta(t_r) = Z(t_r)$, that can be expressed as

$$t_r = \frac{t_1 - \beta_o t_o + \Delta z/c}{1 - \beta_o}. \quad (\text{A5})$$

At the time t_r the moving mirror reaches the position

$$Z(t_r) = z_1^* + \beta_o c \frac{t_1 - t_o + \Delta z/c}{1 - \beta_o}. \quad (\text{A6})$$

Thereafter, photons are propagating back and their position along the z -axis is given by $\zeta(t - t_r) = Z(t_r) - c(t - t_r)$, for a time $t > t_r$.

The plasmoid moving at height $z(t)$ along the z -axis is irradiated by the reflected radiation at time t_C , and the travel-time condition reads now

$$\zeta(t_C - t_r) = z(t_C), \quad (\text{A7})$$

that is,

$$Z(t_r) - c(t_C - t_r) = z_1 + \beta c(t_C - t_1). \quad (\text{A8})$$

By using Eqs. A5 and A6 we find

$$\frac{\Delta z}{c}(1 - \beta_o) + \beta_o(t_1 - t_o + \frac{\Delta z}{c}) + t_1 - \beta_o t_o + \frac{\Delta z}{c} + t_1 \beta(1 - \beta_o) = t_C(1 + \beta)(1 - \beta_o). \quad (\text{A9})$$

Eq. A9 provides the time t_C when radiation hits back the approaching plasmoid for a given value of t_1 . As the emission process is continuous, also the corresponding process of mirroring and IC radiation cover a range of t_C . We stress that the time t_C of the Compton radiation constitutes the abscissa t of the representative gamma-ray lightcurve plotted as Fig. 5. The highest energy densities of the reflected radiation obtain at the time t_C when the shortest distance is attained between the moving mirror at $Z(t_C)$ and the plasmoid following at the position $z(t_C)$. The mirror-plasmoid distance at the time t_C of Compton upscattering is

$$d(t_C) = Z(t_C) - z(t_C). \quad (\text{A10})$$

Before applying Eqs. A9 and A10 in full, we check them on the simple case of a static mirror. Then $\beta_o = 0$ and $z_1^* = R_m$ hold, where R_m is the constant mirror distance from the central black hole; the reflection time is $t_r = \Delta z/c + t_1$. The location of the reflected radiation is $\zeta(t) = R_m - c(t - t_r)$, and the light travel-time condition becomes $\zeta(t_C - t_r) = z(t_C)$. Thus, we obtain $t_C = 2(\Delta z/c)/(1 + \beta) + t_1$, and the plasmoid - static mirror distance $d = R_m - z(t_C) = \Delta z - 2\beta \Delta z/(1 + \beta) = \Delta z(1 - \beta)/(1 + \beta)$, where in this case, $\Delta z = R_m - z_1$. Thus we recover Eq. 1 for $\beta \simeq 1 - 1/(2\Gamma^2)$.

Having checked our formalism, we now apply it in full to the moving mirror case. The mirror-plasmoid distance as a function of time is given in the model considered in this paper by the *linear* dependence

$$d(t) = Z(t) - z(t) = D_{in} - c(t - t_1)(\beta - \beta_o), \quad (\text{A11})$$

where we defined the initial distance at time t_1 as

$$D_{in} = \Delta z + D_o, \quad (\text{A12})$$

in terms of the distance D_o travelled by the mirror during the time interval between mirror and plasmoid transits through the point z_1 , i.e.,

$$D_o = \beta_o c (t_1 - t_o). \quad (\text{A13})$$

From Eq. A10, we derive the mirror-plasmoid distance at time t_C ,

$$d(t_C) = (\beta_o - \beta) c \frac{2 \Delta z + \beta_o(t_1 - t_o) + (t_1 - \beta_o t_o) + t_1 \beta (1 - \beta_o)}{(1 + \beta)(1 - \beta_o)} + \beta c t_1 - \beta_o c t_o + \Delta z. \quad (\text{A14})$$

By adding and subtracting the quantity $\beta_o t_1$ and rewriting Eq. A14 in terms of the initial distance D_{in} we obtain

$$d(t_C) = D_{in} \left[1 + \frac{2(\beta_o - \beta)}{(1 + \beta)(1 - \beta_o)} \right]. \quad (\text{A15})$$

Eq. A15 is our main result for the moving mirror case. We note that for the case $\beta_o = 0$ (static mirror) we obtain $d(t_C) = \Delta z (1 - \beta)/(1 + \beta)$, again in agreement with Eq. 1 considering that, in this case, $\Delta z = z_1^* - z_1 = R_m - R_1$.

For both β_o and β close to unity, we have

$$d \equiv d(t_C) \simeq D_{in} \left[1 + \frac{\beta_o - \beta}{1 - \beta_o} \right]. \quad (\text{A16})$$

A key quantity that can be defined as the effective photon "compression gap" is the distance \tilde{d} between the mirror location at the moment of reflection $Z(t_r)$ and the distance travelled by the plasmoid at the Compton up-scattering event, $z_2(t_C)$, that is

$$\tilde{d} = Z(t_r) - z(t_C), \quad (\text{A17})$$

that can be calculated to be

$$\tilde{d} = D_{in} \left[\frac{(1 - \beta)}{(1 + \beta)(1 - \beta_o)} \right]. \quad (\text{A18})$$

For a static mirror with $\beta_o = 0$, we find $\tilde{d} = D_{in} (1 - \beta)/(1 + \beta) \simeq D_{in}/4\Gamma^2$.

A number of particular cases may be considered:

- for $\beta_o > \beta$, the distance d is larger than D_{in} , making the energy density of reflected radiation ineffective at inducing an intense inverse Compton radiation;
- for $\beta_o = \beta$, the distances d and \tilde{d} are constant and equal a fixed distance $D_{in} = \Delta z = \tilde{R}_m - R_1$;

- for $\beta_o < \beta$, the limiting distances d and \tilde{d} can be substantially smaller than D_{in} , and read

$$d \simeq D_{in} \left[1 + \left(\frac{1}{\Gamma^2} - \frac{1}{\Gamma_o^2} \right) \Gamma_o^2 \right] = D_{in} \frac{\Gamma_o^2}{\Gamma^2}, \quad (\text{A19})$$

$$\tilde{d} \simeq \frac{D_{in}}{2} \left(\frac{\Gamma_o}{\Gamma} \right)^2. \quad (\text{A20})$$

We stress that for $\beta_o = \beta$ the mirror mechanism leads to a constant flux, while for $\beta_o < \beta$ it yields a time variable high-energy flux.

B. Appendix: Photon Densities

The local photon density in the plasmoid comoving frame U' is built up by different radiative contributions as the plasmoid moves outward along the jet. Within the BLR, U' is set by the average soft photon density $U_{BLR} = L_D / 4\pi c R_{BLR}^2$, so that $U' \simeq (4/3)U_{BLR}\Gamma^2$, where Γ is the plasmoid bulk Lorentz factor, and $R_{BLR} \simeq 3 \cdot 10^{17}$ cm (e.g., Dermer & Schlickeiser, 1994). Outside the BLR, i.e., at distances $r \geq R_{BLR}$ along the jet, U' is dominated by the contribution of the dusty torus which has overall luminosity and average photon energies smaller than those within the BLR. Compared with the mirrored synchrotron emission, the latter contribution is less effective in producing GeV gamma-ray flares by inverse Compton up-scattering of IR photons also in view of the Klein-Nishina effects.

A substantial contribution to U' is instead provided by radiation emitted by the plasmoid within the BLR and only partially reflected by a facing mirror at a distance R_m substantially larger than R_{BLR} . Notice that the original radiation flux is only partially captured by the distant mirror at R_m .

Let us first consider a static mirror. Then the fraction of the plasmoid radiation impinging on the mirror is set not only by the flux dilution at the considerable distance between emitter and mirror, but is also proportional to the solid angle $\delta\omega_m \propto \pi r_m^2$ subtended by the mirror of size r_m . Thus the lab-frame luminosity captured by the mirror is

$$L_m \simeq L'_S \frac{\pi r_m^2}{\pi \theta^2 R_m^2} \Gamma^2 \quad (\text{B1})$$

where the factor Γ^2 accounts for the Lorentz transformation of energy and time, and the emitter radiates in the solid angle $\pi \theta^2$ in the lab-frame. In Eq. B1 we used the approximation $R_m - R_1 \simeq R_m$. With the transformation $\theta \sim 1/\Gamma$ applied to relativistic motion, we recover that $L_m \sim (r_m/R_m)^2 L_{obs}$, where $L_{obs} = L'_S \Gamma^4$ is the plasmoid original

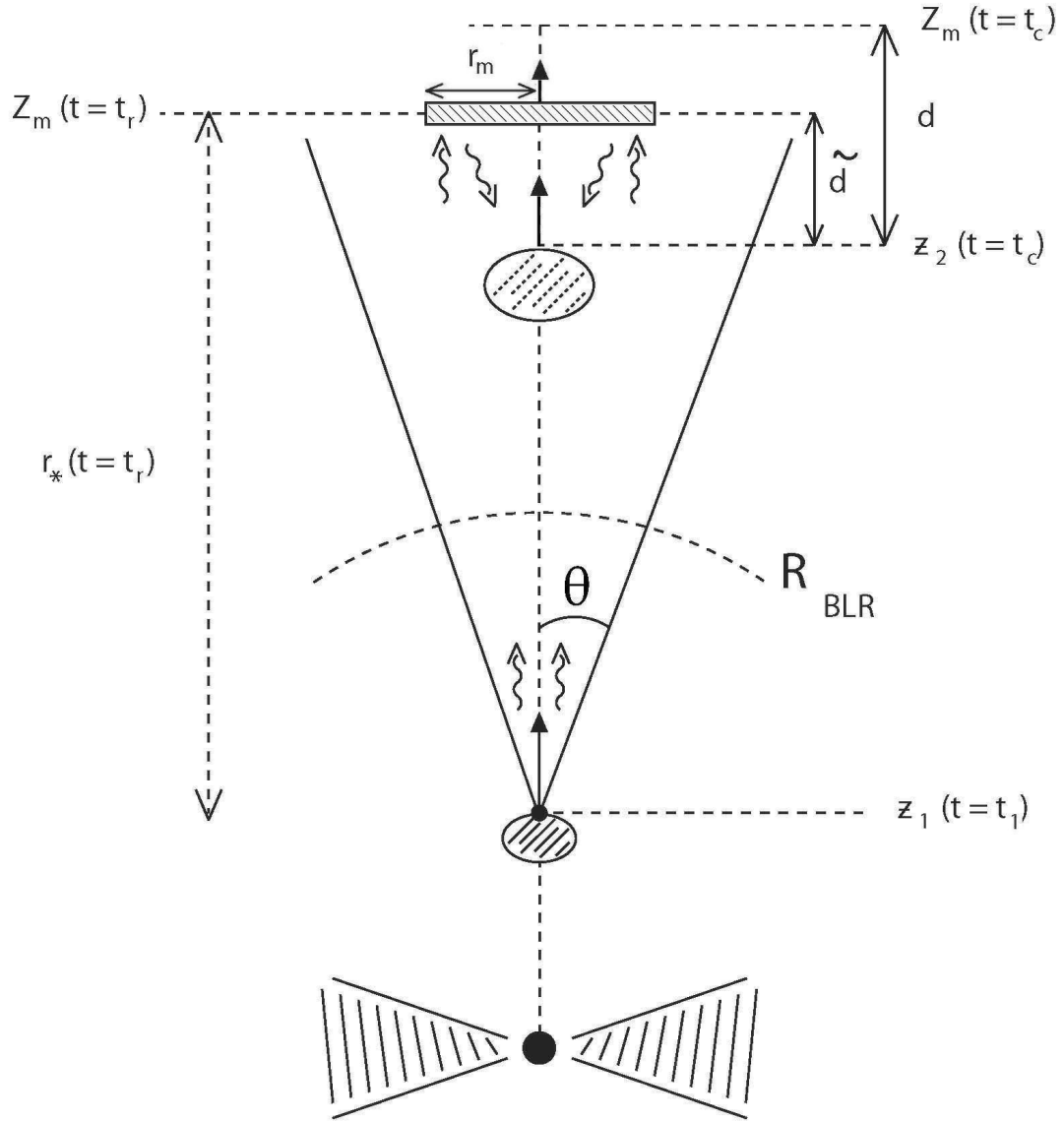


Fig. 7.— Geometry of the kinematic quantities in the moving mirror case (laboratory frame).

luminosity in the observer frame. Eq. B1 assumes $r_m/R_m \leq \theta$ to hold; for $r_m/R_m > \theta$, the usual relation $L_m = L'_S \Gamma^4$ applies.

The mirror reflects the impinging radiation with efficiency f ; at a distance d from the mirror, in the observer frame the energy density of radiation reflected back reads

$$U_m = \frac{f L_m}{2 \pi c d^2}. \quad (\text{B2})$$

In the plasmoid comoving frame the energy density can be written as

$$U'_m = U_m \Gamma^2, \quad (\text{B3})$$

with the quantity (of order unity) η given by Eq. C7 in Appendix C. Thus,

$$U'_m = \frac{f \eta}{2 \pi c} \left(\frac{r_m}{R_m} \right)^2 \frac{L'_S \Gamma^4}{d^2} \Gamma^2. \quad (\text{B4})$$

For a moving mirror the calculation of U' proceeds through steps analogous to the static case, with proper modifications. In the laboratory frame, the energy density of the radiation emitted forward at time t_1 by the plasmoid at height z_1 is, $U(r_*) = L'_S \Gamma^2 / (\pi \theta^2 c r_*^2)$, where L'_S is the initial luminosity in the plasmoid co-moving frame, and r_* is the distance at which the mirror reflection occurs, i.e., in the formalism of the Appendix A, $r_* = Z(t_r) - z_1$, that becomes

$$r_* = [\Delta z (1 + \beta_o) + \beta_o c (t_1 - t_o)] / (1 - \beta_o). \quad (\text{B5})$$

We assumed that in the observer's frame the plasmoid emission is beamed into a forward cone of semi-aperture θ . At time t_r (see Eq. A5 in Appendix A), a fraction f of the impinging luminosity is reflected back by the moving mirror, with luminosity L_m given by $L_m = \pi r_m^2 c f U(r_*)$, where r_m is the plasmoid size, and $f \sim 0.1$. We then have

$$L_m = \pi r_m^2 c f \frac{L'_S \Gamma^2}{\pi \theta^2 c r_*^2} \simeq \frac{f L'_S}{4} \left(\frac{r_m}{D_o} \right)^2 \left(\frac{\Gamma}{\Gamma_o} \right)^4, \quad (\text{B6})$$

where we used the relativistic beaming relation $\theta \sim 1/\Gamma$, and from Eq. B5 with $\Delta z = 0$ and $D_o = \beta_o c (t_1 - t_o)$,

$$r_* = 2 D_o \Gamma_o^2. \quad (\text{B7})$$

Eq. B6 can therefore be used to calculate the photon energy density of the reflected radiation at the "backward" distance \tilde{d} , U_m , that in the laboratory frame for isotropic emission in the backward half-hemisphere is

$$U_m = \frac{L_m}{2 \pi \tilde{d}^2 c}. \quad (\text{B8})$$

Finally, the reflected photon energy density in the plasmoid comoving frame at the moment of Compton up-scattering t_C reads (see also Appendix C and Eq. C7 properly modified for a moving mirror)

$$U'_m = \tilde{\eta} U_m \Gamma_r^2 = \frac{f \tilde{\eta} L'_S}{2 \pi c} \left(\frac{r_m}{D_o} \right)^2 \frac{1}{4} \left(\frac{\Gamma}{\Gamma_o} \right)^4 \frac{1}{\tilde{d}^2} \Gamma_r^2, \quad (\text{B9})$$

where Γ_r is the *relative* Lorentz factor between the moving mirror and plasmoid given by Eq. C8 of Appendix C. For values of $\Gamma_o^2 \gg 1$ and $\Gamma^2 \gg 1$ with $\Gamma > \Gamma_o$, we have $\Gamma_r \simeq \Gamma/2\Gamma_o$ (see Appendix C). Therefore,

$$U'_m = \frac{2 f \tilde{\eta}}{\pi c} \left(\frac{r_m}{D_o} \right)^2 \frac{L'_S \Gamma_r^4}{\tilde{d}^2} \Gamma_r^2. \quad (\text{B10})$$

Note that this last equation for U'_m for the moving mirror case is similar to the static mirror (Eq. B4) except for the kinematic factor $4\tilde{\eta}$, the dependence of d and \tilde{d} on Γ , and the obvious substitution $\Gamma \rightarrow \Gamma_r$. On using Eq. 8 and $\Delta z = 0$, we obtain

$$U'_m = \frac{f \tilde{\eta} L'_S}{2 \pi c} \left(\frac{r_m}{D_o} \right)^2 \frac{1}{D_o^2} \left(\frac{\Gamma}{\Gamma_o} \right)^8 \Gamma_r^2. \quad (\text{B11})$$

In terms of Γ_r we have

$$U'_m = \frac{2^8 f \tilde{\eta}}{2 \pi c} \left(\frac{r_m}{D_o} \right)^2 \frac{L'_S \Gamma_r^4}{D_o^2} \Gamma_r^6. \quad (\text{B12})$$

Note that powers of Γ in Eqs. B11 and B12 appear to be different from those of Eq. B10, but in fact, these equations are consistent once the appropriate definition of the distance \tilde{d} is used (see Eq. A20).

For values that can be reasonably applied to our situation, $r_m \simeq 3 \cdot 10^{16}$ cm, $D_o \simeq 3 r_m$, $f = 0.1 f_{-1}$, and $\Gamma_o = 3$, we have

$$U'_m \simeq (f_{-1} 10^{-7} \text{ erg cm}^{-2}) L'_{S,42} \frac{1}{(\Gamma_o/3)^2} \left(\frac{\Gamma}{\Gamma_o} \right)^8 \Gamma^2, \quad (\text{B13})$$

where $L'_{42} = L'_S/(10^{42} \text{ erg s}^{-1})$.

It is interesting to compare Eq. B13 with a typical photon energy density in the plasmoid comoving frame inside the BLR,

$$U'_{BLR} = \frac{4}{3} \frac{\xi_{BLR} L_D \Gamma^2}{4 \pi R_{BLR}^2 c} \simeq (0.03 \text{ erg cm}^{-3}) L_{D,46} \xi_{BLR,-1} \Gamma^2, \quad (\text{B14})$$

where the disk luminosity is $L_{D,46} = L_D/(10^{46} \text{ erg s}^{-1})$, $R_{BLR} = 3 \cdot 10^{17}$ cm, mtd and $\xi_{BLR} = 0.1 \xi_{BLR,-1}$ is the BLR average covering factor. Note that $U'_m > U'_{BLR}$ for

$$\frac{\Gamma}{\Gamma_o} \gtrsim 4. \quad (\text{B15})$$

Therefore, a plausible configuration for the moving mirror-plasmoid geometry is obtained by the following parameters: $\Gamma \simeq 10 - 15$, $\Gamma_o \simeq 2 - 3$, $r_m \simeq 3 \cdot 10^{16}$ cm.

C. Appendix: Angular Factors

In this Appendix we calculate the angular factor η of the photon energy density U' in the plasmoid comoving frame that is dependent on the mirror-plasmoid distance d . Unprimed quantities are calculated in the laboratory frame; primed quantities refer to the plasmoid comoving frame.

Let us first obtain angular factor η for a static mirror. Denoting by $U_m = L_m/2\pi c d^2$ the photon energy density at a distance d generated by the mirror reflection, we calculate U' by integrating over the specific energy density $U_m/2\pi$,

$$U' = U_m \int_{\mu'_1}^{\mu'_2} \frac{d\mu'}{\Gamma^4(1 + \beta\mu')^4} = U_m \int_{\mu_1}^{\mu_2} \Gamma^2(1 - \beta\mu)^2 d\mu \quad (\text{C1})$$

where the energy Lorentz transformation reads $\epsilon = \Gamma \epsilon' (1 + \beta\mu')$, $\epsilon' = \Gamma \epsilon (1 - \beta\mu)$, and μ and μ' are the direction cosines in the laboratory and comoving frames, respectively (related by $\mu' = (\mu - \beta)/(1 - \beta\mu)$). In our case

$$U' = U_m \int_{-1}^{-\mu^*} \Gamma^2(1 - \beta\mu)^2 d\mu = U_m \Gamma^2 \left[-\frac{1}{3\beta} (1 - \beta\mu)^3 \right]_{-1}^{-\mu^*} \quad (\text{C2})$$

with μ^* the upper extreme of integration that depends on the relative sizes of r_m vs. d , i.e.,

$$\mu^* = \frac{d}{\sqrt{r_m^2 + d^2}}. \quad (\text{C3})$$

By defining $\beta_d = \beta \mu^*$, we have

$$U' = U_m \frac{1}{3\beta} \Gamma^2 [(1 + \beta)^3 - (1 + \beta_d)^3]. \quad (\text{C4})$$

We can then define the function η that takes into account the angular integration in the calculation of U' ,

$$U' = \eta U_m \Gamma^2, \quad (\text{C5})$$

with

$$\eta = \frac{1}{\beta} \left[\beta - \beta_d + \beta^2 - \beta_d^2 + \frac{1}{3} (\beta^3 - \beta_d^3) \right], \quad (\text{C6})$$

which can be rewritten as

$$\eta = 1 - \mu_* + \beta(1 - \mu_*^2) + \frac{1}{3}\beta^2(1 - \mu_*^3). \quad (\text{C7})$$

For a moving mirror, the calculation of the angular factor proceeds in a similar way, with the replacements in the above expressions: of $\eta \rightarrow \tilde{\eta}$, $d \rightarrow \tilde{d}$, $\beta \rightarrow \beta_r$, and $\Gamma \rightarrow \Gamma_r$; β_r and Γ_r are related by the usual relation $1 - \beta_r^2 = 1/\Gamma_r^2$. The quantity Γ_r is the relative bulk Lorentz factor between mirror and plasmoid and is obtained by the Lorentz transformation in the mirror frame

$$\Gamma_r = \Gamma \Gamma_o (1 - \beta \beta_o). \quad (\text{C8})$$

It is useful to note that for $\Gamma^2 \gg 1$, $\Gamma_o^2 \gg 1$, we can approximate the relative Lorentz factor as

$$\Gamma_r \simeq \frac{1}{2} \left(\frac{\Gamma}{\Gamma_o} + \frac{\Gamma_o}{\Gamma} \right). \quad (\text{C9})$$

For $\Gamma > \Gamma_o$, the simple approximation $\Gamma_r \simeq \Gamma/2\Gamma_o$ can be used.